NISTIR 6222

A Molecular Dynamics Study of a Reversed-Phase Liquid Chromatography Model

Joseph T. Slusher
Raymond D. Mountain

U.S. DEPARTMENT OF COMMERCE
Technology Administration
Physical and Chemical Properties Division
National Institute of Standards
and Technology
Gaithersburg, MD 20899-0001

NIST

NISTIR 6222

A Molecular Dynamics Study of a Reversed-Phase Liquid Chromatography Model

Joseph T. Slusher
Raymond D. Mountain

U.S. DEPARTMENT OF COMMERCE
Technology Administration
Physical and Chemical Properties Division
National Institute of Standards
and Technology
Gaithersburg, MD 20899-0001

September 1998

U.S. DEPARTMENT OF COMMERCE
William M. Daley, Secretary

TECHNOLOGY ADMINISTRATION
Gary R. Bachula, Acting Under Secretary
for Technology

NATIONAL INSTITUTE OF STANDARDS
AND TECHNOLOGY
Raymond G. Kammer, Director

A Molecular Dynamics Study of a Reversed-Phase Liquid Chromatography Model

Joseph T. Slusher and Raymond D. Mountain

Physical and Chemical Properties Division
National Institute of Standards and Technology
Gaithersburg, MD 20899

We describe a molecular dynamics simulation study of a model of the reversed-phase chromatographic system. The model consists of a slab of aqueous solvent sandwiched between two walls having attached C_8 hydrocarbon chains at a surface coverage of 5.09 μmol/m^2 or 32.6 $\AA^2$/chain. Long-ranged Coulombic interactions are taken into account using the Ewald sum method of Rhee, et al. [Phys. Rev. B, 40, 36, 1989]. The density, energy, pressure, and solvent orientation profiles are computed as a function of distance from the walls. The presence of an organic co-solvent methanol or acetonitrile at 30.8 mole % has little effect on the chain structure, which is largely collapsed against the walls. We also estimate the change in residual Helmholtz free energy along the pore width for a methane solute in the acetonitrile/water system, which indicates that a substantial portion of the free energy driving force for retention occurs in an organic-rich layer of solvent adsorbed to the hydrocarbon phase.

1 Introduction

The retention mechanism in reversed phase liquid chromatography (RPLC) is an important problem in measurement technology which has received considerable attention in recent years [1, 2]. A number of experimental methodologies have been brought to bear on the problem with varied and sometimes conflicting results [3]. The continuing interest in this area reflects the substantial difficulty in understanding the behavior (and thus our ability to predict/optimize) in these systems, which arises, in large part from the inherent complexity in RPLC systems. One must address, in addition to state variables (*i.e.* temperature, pressure, flow rate), additional variables such as ligand density, chain length, and mobile phase composition, as well as the nature of the solute. Other important quantities, which are often unknown, are the surface coverage of exposed silanol groups [4, 5, 6] and the uniformity in surface density of the stationary alkyl chains [7]. A further difficulty in the analysis arises in the use of bulk thermodynamic treatments to describe a situation which is inherently interfacial [8].

Some of the major questions which have been addressed have concerned the role of solvophobic *vs.* chain-solute interactions [9], the relative importance of partitioning *vs.* adsorption [10], the degree of solvent penetration into the stationary phase [11], and the effect of the presence of microheterogeneities [12, 13] or 'layering' in mixed-solvent mobile phases [14]. Solute shape selectivities in relation to bonded-phase densities have also been addressed experimentally [11, 15, 16].

A fruitful area of inquiry has dealt with the underlying bases for the different behavior seen in two commonly used RP mobile phases, aqueous methanol and aqueous acetonitrile. Here, thermodynamic measurements from van't Hoff plots of the mobile-phase composition dependence of the enthalpy ($\Delta H°$) and entropy ($\Delta S°$) of solute transfer (from mobile to stationary phases) show marked qualitatively different characteristics between the two systems. For instance, with aromatic solutes, several groups [12, 17, 18] have found that both $\Delta H°$ and $\Delta S°$ decrease monotonically with increasing water volume fraction (θ_w) for the methanol/water system. In acetonitrile/water sytems, $\Delta H°$ is independent of θ_w while $\Delta S°$ increases with increasing θ_w for $\theta_w < 0.5$. As a decrease in $\Delta H°$ indicates an increasing energetic preference while a decrease in $\Delta S°$ indicates a decreasing entropic preference for the stationary phase, these experiments suggest, for the acetonitrile system, an entropically governed retention process for $\theta_w < 0.5$. The molecular picture which emerges from the experimental results is one in which the solute is solvated by acetonitrile-rich pockets which exist in the water-poor mobile phase [12, 19, 20, 21]. Hanai *et al.* have found similar trends in $\Delta H°$ and $\Delta S°$ for various other non-polar solutes [22]. The microheterogenious nature of acetonitrile/water mixtures at ambient temperatures has been indicated experimentally via Raman spectroscopy [23] as well as inverse Kirkwood-Buff studies [24], and is not surprising in view of the rather high upper critical solution temperature (272 K) [19] and the expectation of strong dipole-dipole interactions between acetonitrile molecules due to their linear shape and the relatively large dipole moment of acetonitrile (3.9 D) [25]. In contrast to the acetonitrile/water system, enthalpic contributions to solute transfer are observed to dominate in the methanol/water systems [12]. Such comparitive studies have contributed greatly to our overall understanding of the retention process in RPLC.

An important piece of information related to the retention mechanism in RPLC is the distribution of the solvent species in the vicinity of the stationary phase, where layering of both the alkyl chains and the mobile phase components is generally acknowledged. The preferential adsorption or intercalation of the organic component has been implicated in significant changes in the ordering of the stationary phase [13, 26]. As it relates to $\Delta S°$, such relative ordering effects in the stationary phase are likely to have a strong influence on the retention driving force [27, 28]. In this regard, there are once again distinctly different mobile phases-stationary phase association characteristics between aqueous methanol and aqueous acetonitrile mobile phases [13, 29]. Here, experimental evidence suggests that association between methanol and the stationary phase increases weakly with bulk methanol solvent composition, whereas that of acetonitrile saturates early and remains fairly constant. These authors also found differences in the association of water with the stationary phase between the two systems.

Molecular dynamics (MD) simulations offer the interesting possibility of addressing in a detailed way some of the molecular inferences suggested by the experimental measurements, under the assumption that the model system correctly captures the key features of the actual system. Recently, Klatte and Beck [30] used MD simulation to probe the driving forces that govern the retention process of a small non-polar solute (methane) in a model system of 50/50 (v/v) water/methanol with a C_{18} stationary phase. Their results, though not unambiguous, support an interfacial rather than a bulk partitioning view of the retention process, where the bulk of the driving force is located at a methanol-rich layer at the interface. In the present work, we develop a similar MD model of the RPLC system in which we compare the solvation structure in a pure water system, a methanol/water system, and an acetonitrile/water system. The long-ranged goal of this work is to examine some of the

features of these systems responsible for the retention mechanism, and to gain insight into the molecular picture of the microscopic differences in solvation structure among the three systems. It should be noted that the current approach ignores the nonequilibrium nature of an actual chromatographic process by disregarding the flow field and its effects. This approach is necessary because the time-scale disparity between a typical flow velocity and the currently achievable length of a MD simulation is very large so that only simulations at equilibrium conditions are possible. However, insight into the equilibrium driving forces for retention and the mechanisms for solute selectivity is a foundational step toward a full understanding of solute retention in RPLC.

In the following section, the system model is described followed by a discussion of the technical details. In section three we discuss the computation of changes in chemical potential of an infinitely dilute solute as a function of distance from the wall. And finally, simulation results are presented for the z-dependence of the density, energy, pressure, solvent orientation and free energy, and some chain structure results.

2 Models and Simulation Methodology

The system under study is a quasi-2-dimensional (2DP) one, with periodicity in the x and y directions but finite in the z direction, which is bounded by two 'walls' representing the silica surface of the pore. The total potential energy of the system consists of *intermolecular* contributions from solvent-solvent, solute-solvent, solvent-chain, solute-chain, and chain-chain, and *intramolecular* contributions in the chains. There are also interactions between all the molecules in the cell and both walls, and a spring-like interaction which attaches the C_8 chains to the wall. With the exception of the latter, all of the interactions are of the Lennard-Jones (LJ) form, with the addition of Coulombic terms for the solvent-solvent interactions.

For the purpose of our study, (and although we are aware that the molecular details of the silica may not be unimportant), due to the lack of a generally available potential for silica we have chosen to model the walls using an integrated 10-4 Lennard-Jones (LJ) potential [31],

$$U^{wall} = 2\pi\varepsilon_w \left\{ 0.4 \left(\frac{\sigma_w}{z}\right)^{10} - \left(\frac{\sigma_w}{z}\right)^{4} - \frac{C_1}{(z/\sigma_w + C_2)^3} \right\}, \tag{1}$$

where $C_1 = 0.47140452$ and $C_2 = 0.431335136$ are constants, and ε_w and σ_w are taken as ε_{OO} and σ_{OO} of the water model. The neglect of the wall details is probably a reasonable approximation for the relatively high surface coverage studied here and particularly for the specific case of a nonpolar solute, which would not be expected to interact appreciably with any exposed silanol groups. The C_8 chains are modeled in the united-atom approximation, including both bending and torsion (but not stretching), and a self interaction using the Lennard Jones potential between sites more than 3 bonds apart [32]. The bending potential is given by [33]

$$U^{bend}(\theta) = \frac{1}{2} c_\theta (\theta - \theta_\circ)^2, \tag{2}$$

where c_θ/k_b is 3.018846×10^4 K/rad^2 and $\theta_\circ = 109.5°$. The torsional potential acts on 5 sets of 4 sites within a C_8 chain, and is given by [32]

$$U^{tors}(\phi) = \sum_{k=0}^{5} c_k (\cos\phi)^k, \tag{3}$$

where ϕ is the dihedral angle defined so that $\phi = 0$ corresponds to the *trans* configuration, and the constants c_k are $c_0/k_b = 1.116 \times 10^3$ K, $c_1/k_b = 1.462 \times 10^3$ K, $c_2/k_b = -1.578 \times 10^3$ K, $c_3/k_b = -3.68 \times 10^2$ K, $c_4/k_b = 3.156 \times 10^3$ K, and $c_5/k_b = -3.788 \times 10^3$ K. The intramolecular forces arising from the torsional interaction acting on contiguous sites i, j, k, and l have been derived following the development of Bekker, et al., [34],

$$\mathbf{F}_i^{tors} = -\nabla_{\mathbf{r}_i} U^{tors} = -\frac{dU^{tors}}{d\phi}\frac{\partial\phi}{\partial\mathbf{r}_i}, \tag{4}$$

where

$$\phi \equiv \text{sign}(\phi)\cos^{-1}(\hat{\mathbf{R}}\cdot\hat{\mathbf{S}}) \tag{5}$$
$$\mathbf{R} \equiv \mathbf{r}_{ij} - (\mathbf{r}_{ij}\cdot\hat{\mathbf{r}}_{kj})\hat{\mathbf{r}}_{kj} \tag{6}$$
$$\mathbf{S} \equiv \mathbf{r}_{lk} - (\mathbf{r}_{lk}\cdot\hat{\mathbf{r}}_{kj})\hat{\mathbf{r}}_{kj} \tag{7}$$
$$\mathbf{r}_{ij} = \mathbf{r}_i - \mathbf{r}_j, \qquad \hat{\mathbf{r}} = \mathbf{r}/|\mathbf{r}|, \tag{8}$$

and where sign(ϕ) is the sign of the quantity $\mathbf{r}_{ij}\cdot\mathbf{n}$. In the above equations, $\mathbf{R}$ and $\mathbf{S}$ are vectors normal to $\mathbf{r}_{kj}$ in the planes defined by the positions of sites i, j, k, and j, k, l, respectively. The vectors $\mathbf{m}$ and $\mathbf{n}$ are normal to the planes defined by sites i, j, k and j,k, l, and have the same direction when sites i, j, k, and l are coplanar:

$$\mathbf{m} \equiv \mathbf{r}_{ij}\times\mathbf{r}_{kj} \tag{9}$$
$$\mathbf{n} \equiv \mathbf{r}_{kj}\times\mathbf{r}_{lk}. \tag{10}$$

With the above definitions, and using the fact that $\mathbf{F}_i + \mathbf{F}_j + \mathbf{F}_k + \mathbf{F}_l = 0$, the torsional forces are given by [34]

$$\mathbf{F}_i = -\frac{du^{Rot}(\phi)}{d\phi}r_{kj}\frac{\mathbf{m}}{\mathbf{m}\cdot\mathbf{m}} \tag{11}$$
$$\mathbf{F}_l = -\frac{du^{Rot}(\phi)}{d\phi}r_{kj}\frac{\mathbf{n}}{\mathbf{n}\cdot\mathbf{n}} \tag{12}$$
$$\mathbf{F}_j = -\mathbf{F}_i + \left(\frac{\mathbf{r}_{ij}\cdot\mathbf{r}_{kj}}{r_{kj}^2}\right)\mathbf{F}_i - \left(\frac{\mathbf{r}_{kl}\cdot\mathbf{r}_{kj}}{r_{kj}^2}\right)\mathbf{F}_l \tag{13}$$
$$\mathbf{F}_k = -\mathbf{F}_l - \left(\frac{\mathbf{r}_{ij}\cdot\mathbf{r}_{kj}}{r_{kj}^2}\right)\mathbf{F}_i + \left(\frac{\mathbf{r}_{kl}\cdot\mathbf{r}_{kj}}{r_{kj}^2}\right)\mathbf{F}_l \tag{14}$$

The chains are fixed to the wall with an arbitrary spring potential having a stiff constant, acting between a position approximately 3 $\AA$ from the wall and the first site of the chain, r_1,

$$U^{spring} = c_{spring}(r_1 - r_\circ)^2, \tag{15}$$

with $c_{spring}/k_b = 2.27 \times 10^4$ K/Å^2. In an attempt to mimic the assumed roughness of the surface of the silica pore, the chains are allowed to move freely in the x, y, and z directions for about 0.5 - 1 ps before fixing the locations of the end sites at $r_\circ$. The resulting positions of $r_\circ$ were within 3 ± 1.5 $\AA$ from the wall.

For the solvent water, we adopt the SPC potential [35], for methanol the potential parameters of van Leeuwen [36], and for acetonitrile the model of Edwards *et al.* [37]. The parameters for the intermolecular potentials are collected in Tables I and II. For unlike sites,

Table I: Geometrical parameters for molecular models

molecule	bond	length (nm)	bond-angle	degrees
SPC water	O-H	0.1008	HOH	109.47
L1 methanol	C-O	0.14246	COH	108.53
	O-H	0.09451		
acetonitrile	CH_3-C	0.146		
	C-N	0.117		
C_8	C-C	0.153	CCC	115.0

Table II: Pair potential parameters

molecule	group	σ (nm)	ε/k_b (K)	q
SPC water	O	0.3166	77.92	-0.820
	H	0	0	0.410
L1 methanol	O	0.303	86.5	-0.700
	CH_3	0.3740	105.2	0.265
	H	0.00	0.000	0.435
acetonitrile	CH_3	0.360	191.0	0.269
	C	0.340	50.0	0.129
	N	0.330	50.0	-0.398
C_8	CH_n	0.396	72.9558	0.000

the Lennard-Jones parameters are obtained via the usual Lorentz-Berthelot combining rules, *i.e.*, $\sigma_{\alpha\beta} = (\sigma_\alpha + \sigma_\beta)/2$, and $\epsilon_{\alpha\beta} = (\epsilon_\alpha \epsilon_\beta)^{1/2}$.

The system contained a total of 500 solvent molecules and 50 C_8 chains, of half of which are attached to each wall. The equations of motion were solved using non-iterative constraint dynamics [38] with the Beeman algorithm [39] and a Nosé-Hoover thermostat [40] to control the temperature.

2.1 Technical Issues

In Coulombic systems having broken symmetry in one direction, it has been shown that the use of the usual formulation of the Ewald sum for 3-dimensional periodicity (3DP) is inappropriate [41, 42]. This is true because use of the 3DP formulation in a system having 2D periodicity in the x and y directions, but which is finite in the z direction, would introduce spurious effects of charge layers perpendicular to the z direction which are not part of the system. Thus, in order to rigorously deal with the long-ranged Coulombic interactions in such a system, an alternate Ewald-like method must be used. A recent review of some of these approaches can be found in reference [43]. Generally, a particular method is computationally feasible within only a rather narrow geometric arrangement of the charges. Outside of this range, the methods either contain singularities or begin to converge very slowly. For instance, the recent method of Hautman and Klein [44] converges slowly for a given $x-y$-direction side length L when z/L becomes large (*i.e.* close to 1). This particular method also depends on inverse powers of the $x-y$ distance s, which can also cause numerical difficulties when two charges are stacked in the z-direction. An alternative approach derived by Leckner [45] appears to contain singularities when two of the three coordinate distances approach zero. A method which does not suffer from charge geometry convergence problems has been proposed by Heyes *et al.* [46]. However, because of a complicated z dependence in the Fourier part, this formulation is exceedingly slow. No particular method has emerged as clearly the best approach for the general simulation. We have chosen to use the method proposed by Rhee *et al.* [41], which combines an Ewald-like sum with a multi-pole expansion in the z direction. Although this method unfortunately suffers from one of the same problems as does the Hautman-Klein method, *i.e.*, poor accuracy when the z separation becomes larger than L, it has an advantage over the latter in that it does not depend on inverse powers of s. Both the Rhee *et al.* and the Hautman-Klein methods enjoy a further numerical advantage by eliminating the z dependence in the Fourier part of the sum, allowing it to be factored. Relative to the usual 3DP Ewald sum, however, the computational requirements for the Rhee *et al.* method (as well as the others) are increased by, at the least, approximately an order of magnitude, in the present case because of the necessity of including the layer of cells around the central cell in the real-space sum. For the sake of completeness, we include in the Appendix the expressions for the Coulombic energy and force for the multi-site molecular case, and derive expressions for the pressure tensor in both the 'atomic' and 'molecular' frameworks.

2.2 Numerical Accuracy of Coulombic Interactions

Although the use of the above Ewald sum is numerically expensive, neglect of the long-ranged forces can have a large effect on the accuracy of the Coulombic contribution to the forces. In Figure 1, we compare the accuracy in the forces for two different schemes: spherical cutoff

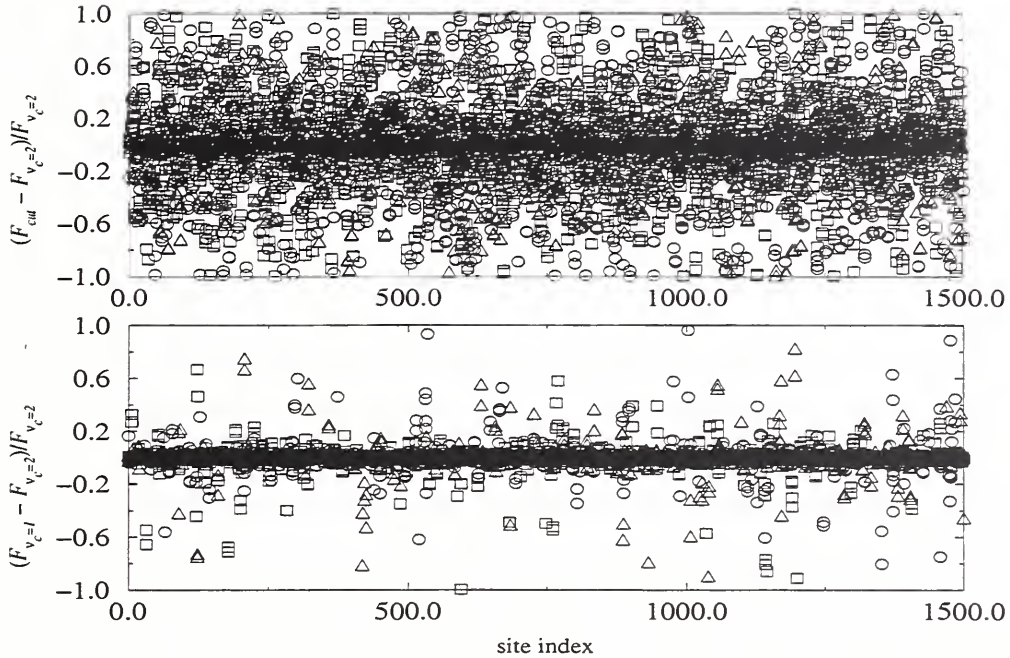

Figure 1: Error in Coulombic contribution to site-site forces with spherical cutoff (TOP) vs. Ewald sum ($\nu = 1$) (BOTTOM) in the x (◯), y (□), and z (△) directions for a typical configuration in the water/C_8 system.

based on site-site minimum image (MI) distances, and the Rhee *et al.* Ewald formulation with a real-space MI site-site cutoff at $\nu_c = 1$, (*i.e.*, nine cells in the real-space sum) and $\alpha/L = 0.1$. The forces are normalized to the essentially exact results found when $\nu_c = 2$. The results are shown for a snapshot configuration from the pure water system, where the effective ration of L_z to L is about 0.92 due to the exclusion of water from near the walls by the hydrocarbon chains. In both cases, the contribution to the forces from the multipole expansion is included. The average absolute errors in the forces with the Ewald sum ($\nu_c = 1$) are 0.72 %, 0.73 % and 0.65 % for the x, y, and z directions. The corresponding errors for spherical cutoff are very large: 33 %, 31 % and 20 %.

2.3 Parallelization

An analysis of the 2DP Ewald sum given in the Appendix reveals that the ordinary time-saving applications of the neighbor-list and/or link-cells [47] cannot be used, a consequence of the fact that no intermolecular cutoff length can be invoked in the evaluation of the real-space part of the Ewald sum without introducing convergence problems. Furthermore, the necessity of including an additional layer of images around the central cell, *i.e.*, 9 more cells, means that the computational requirements are much higher with the present method as compared to the 3DP Ewald sum. In fact, in order to make the computations feasible on presently available machines, the code must be parallelized. Because we are dealing, at present, with relatively small system sizes, and the problem is simply to speed the code, the so-called 'data-replication' scheme is used rather than a domain decomposition. The former involves distribution of the work-load to the various processors, then a global summation of the data at the end of each time-step. In practice, only the force calculation needs to be

parallelized since it accounts for more than 90 % of the work. The routine for calculating the intermolecular forces also calculates the intermolecular potential energy and pressure contributions.

Calculation of the real-space part of the Ewald sum and the short-ranged LJ pair interactions involves a double loop over N molecules i and j, which takes most of the CPU time for the forces:

```
DO I = 1,N-1
 DO J = I+1,N
   calculate pair potentials and pair forces...
 ENDDO
ENDDO
```

The total number of interactions which must be considered in this double loop is $N(N-1)/2$. If the outer loop over i is broken down into say, $K = 4$ chunks of equal size, then the number of interactions considered by the kth chunk is $\frac{N}{4}(N + (k-1)\frac{N}{4}) - \sum_{i=1}^{N/4} i$. The total sum of the interactions considered by chunks $(k = 1) + (k = 4)$ will equal the sum of interactions in chunks $(k = 2) + (k = 3)$, so with 4 chunks the total work in the double loop over i and j can be divided *exactly* over $N_p = 2$ processors, and in general over $N_p = K/2$ processors, as long as N/K is an even integer. The same load-balancing scheme can be modified for use with arbitrary number of processors and arbitrary N, dividing the 'left-over' work over some of the processors.

The work done in calculating the reciprocal space terms in the Ewald sum, which accounts for a significant portion of the total CPU time for the forces, is straightforwardly load-balanced by simply dividing the loop over the reciprocal lattice vectors $\mathbf{h}$ into N_p equal-sized chunks assigned to each processor. In both real and reciprocal calculations, a global sum of the pair forces, energies, virials, etc. must be made at each time-step of the simulation. This is an unavoidable message-passing overhead which effectively limits the number of processors which can be utilized to about 10 for the system sizes considered in this work.

The message passing interface (MPI) library was used in the global summation of the forces, energies, etc. in order to allow portability to various architectures. From the timings for various numbers of processors on an IBM SP2 (at NIST), shown in Figure 2, it can be seen that nearly linear speed-up is obtained for up to 10 processors. Above this number, message-passing overhead begins to dominate the timings.

3 Free Energy Profile

The change in free energy of a solute as it experiences different microenvironments in a RPLC column is the basic driving force in the retention process. In this way, the solute acts as a probe to determine whether the retention is primarily driven by solute-solvent interactions or interactions between the solute and the stationary phase, and whether the process is primarily an interfacial one or if it resembles a bulk partitioning process. The simulation results of Klatte and Beck [30] suggest, at least for small, spherical, non-polar solutes that the process is largely interfacial. For non-spherical solutes, free energy profiles obtained from MD simulations can be used to test ideas such as the slot model [48] and the effects of stationary-phase surface coverage on the partioning. The information we seek is the change in free energy, in this case the residual Helmholtz free energy, of a solute A^{res} at infinite dilution in the model RPLC system, as a function of distance along the z coordinate.

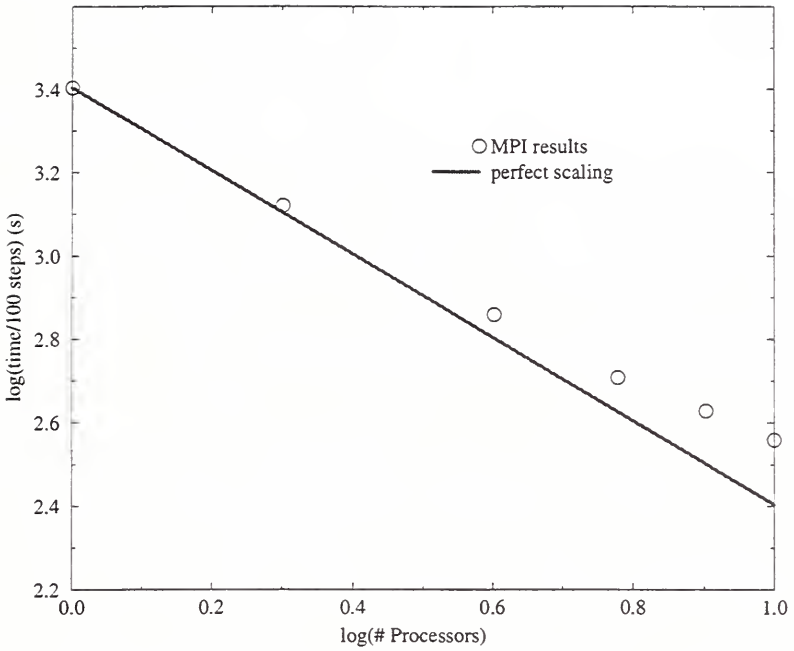

Figure 2: Wall-clock time needed to integrate through 100 timesteps using different numbers of processors, for the system of 500 water molecules with 50 C_8 chains.

The z dependence of the Helmholtz free energy could be calculated from the z dependence of the partition function,

$$A^{res}(z) = -k_b T \ln Q(z), \tag{16}$$

and then relating the z-dependence of the partition function to the probability of finding the solute at a specific z position within the simulation cell. However, such an approach would suffer from extremely poor statistics since the range of possible z values is large and we have only one solute molecule. To overcome this problem, we adopt a commonly used umbrella sampling scheme [49] where the position of the solute is constrained to lie within a certain window of z values. In this case, the configurational energy of the solute is due to solute-solvent, solute-chain, and solute-wall interactions, plus the well potential. The $z-$position of the solute is constrained to lie within a narrow range of z by applying a well potential to the the center of mass or a site near the center of the molecule,

$$U^{well}(z; z_o) = \varepsilon_z \left(\frac{z - z_o}{\sigma_z} \right)^{12}, \tag{17}$$

with arbitrarily chosen values $\sigma_z = 0.7675\mathring{A}$ and $\varepsilon_z/k_b = 8.553 \times 10^4$ K. The solute is then allowed translational freedom in the x and y directions as well as rotational freedom. Within the window, the $z-$dependent free energy is

$$\begin{aligned} A^{res}(z) &= -k_b T \ln Q(z) \\ &= -k_b T \ln \left[e^{-\beta U^{well}(z;z_o)} \int \cdots \int e^{-\beta U(r_{1x}, r_{1y}, z, \vec{r}_2, \ldots, \vec{r}_N)} dr_{1x} dr_{1y} d\vec{r}_2 \cdots d\vec{r}_N \right] \\ &= -k_b T \ln P(z) Q e^{-\beta U^{well}(z;z_o)} \\ &= -k_b T \ln P(z) - k_b T \ln Q + U^{well}(z; z_o), \end{aligned} \tag{18}$$

Table III: State point and configurational energy

System	N_o	N_w	N_{chain}	L (nm)	L_z (nm)	T (K)	P (MPa)[a]	U^c (kJ/mol)[a]	τ^b (ps)
ACN	154	346	50	2.855	4.789	305.9	83(3)	-36.1(1)	403
MeOH	154	346	50	2.855	4.544	298.0	-2(3)	-36.6(1)	371
Water	0	500	50	2.855	3.838	298.0	18(5)	-37.5(1)	258

[a]Standard uncertainty in last digit given in parentheses.
[b]Simulation length.

Table IV: Conditions at center of pore

System	ρ_o (g/cm^3)	ρ_w (g/cm^3)	P (MPa)	x_o^a
ACN	0.252	0.692	80	0.138
MeOH	0.297	0.633	24	0.209
Water	–	1.011	61	–

where $P(z)$ is the probability of finding the solute at a position z within the window. Since we are only concerned with changes in A^{res} with z we can ignore the term $k_bT \ln Q$ in the last equation since it does not depend on z. In practice, $A^{res}(z)$ is calculated for a number of contiguous windows. The total free energy profile is then constructed by requiring the free energy to be the same at the overlap between two windows.

4 Results and Discussion

Table III lists the relevant details of the simulations and some of the computed thermodynamic properties at the center of the slit pore are given in Table IV. No attempt has been made to include long-ranged corrections to the Lennard-Jones contributions for any of the computed properties.

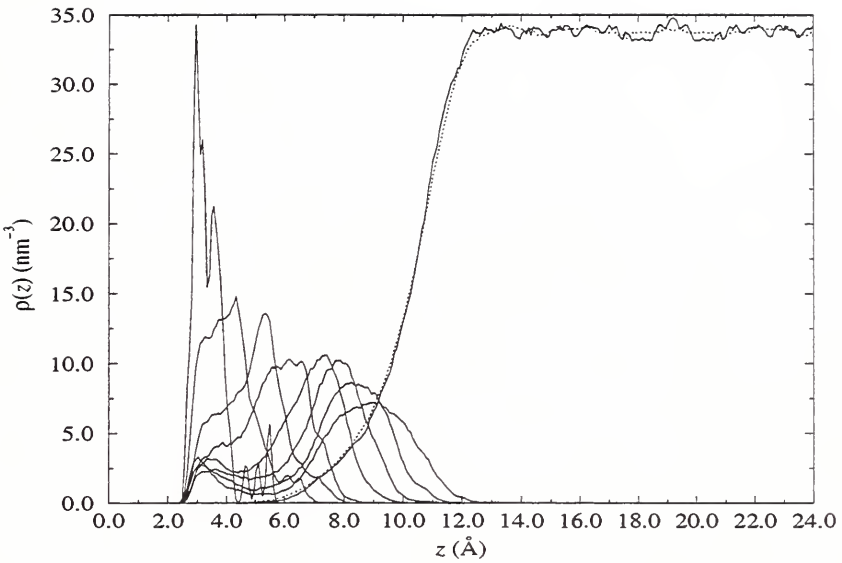

Figure 3: Number density of oxygen (solid line) and hydrogen (dotted line) as a function of z for the pure water system.

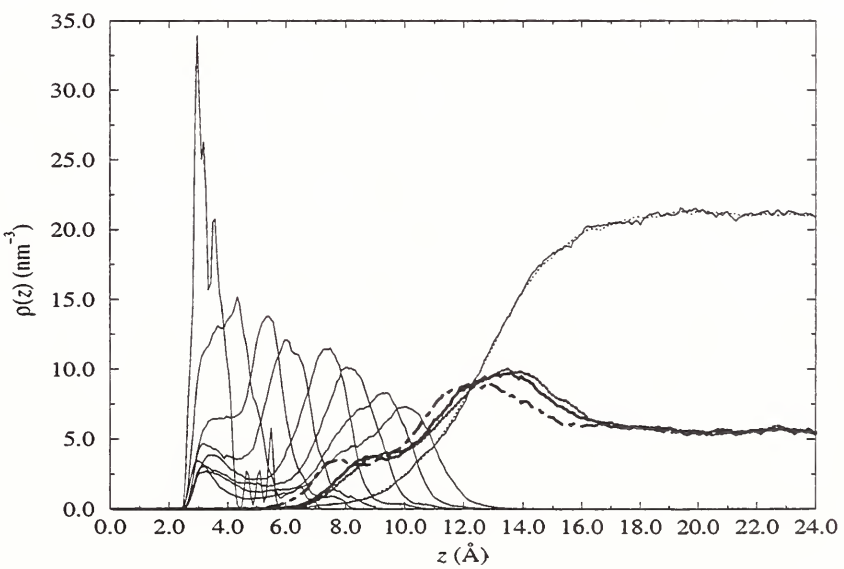

Figure 4: Number density for methanol (bold lines) and water (thin lines) as a function of z for the methanol/water system. CH_3 (dot-dashed), O (solid), and H (dotted).

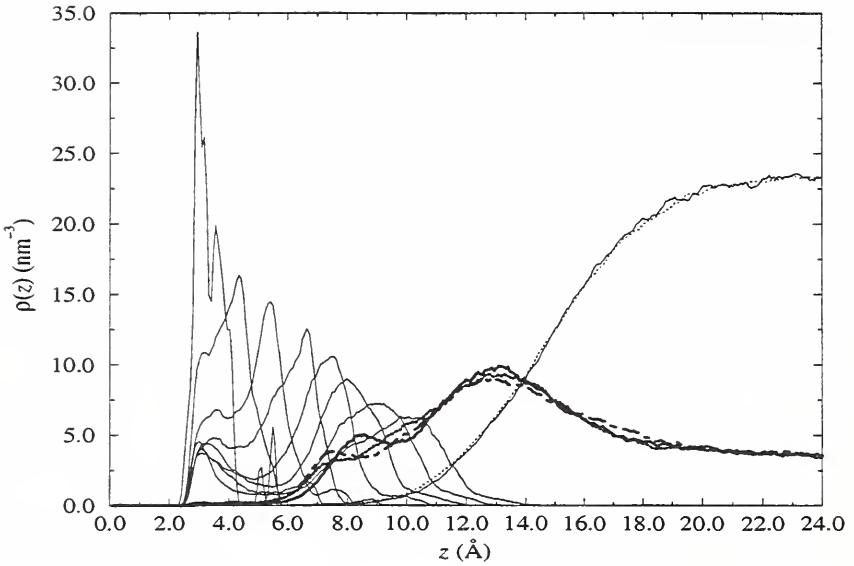

Figure 5: Number density for acetonitrile (bold lines) and water (thin lines) as a function of z for the acetonitrile/water system. CH_3 (dot-dashed), C (solid), and N (dotted).

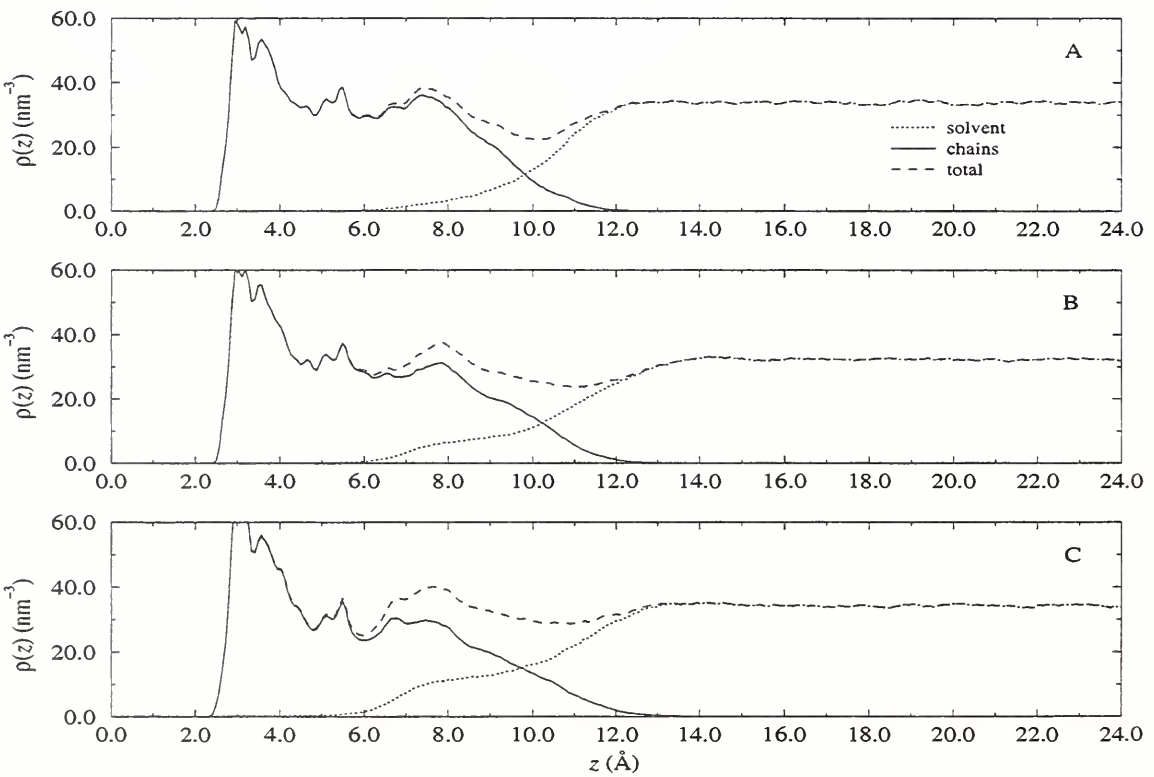

Figure 6: Total density of LJ interaction sites as a function of z for the pure water system (A), methanol/water sytem (B), and acetonitrile/water sytem (C).

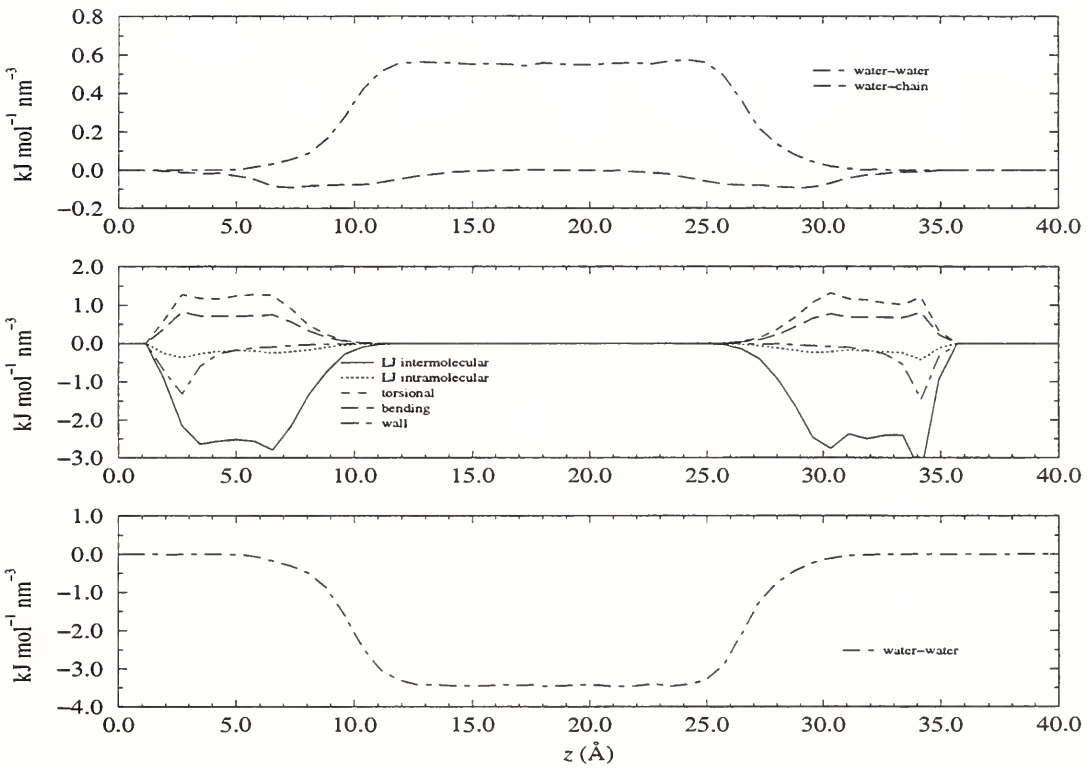

Figure 7: Energy density from various sources as a function of z for the pure water system. Top: LJ, Middle: chain-chain, Bottom: real-space + multipole part of Coulombic. These values were computed using a bin width of 0.7675 $\AA$, giving a volume of each slice of 0.62563 nm^3. Unlike pair energies between molecules i and j are normalized by the total moles of i + j. Like pair energies are normalized by the total moles of i.

4.1 Density profiles

The site density profiles have been computed using a bin width of 0.07675 $\AA$ and are shown in Figures 3 - 5 for the three different systems. In the pure water system, the interface between the water and alkyl chain phases is fairly sharp although there is some degree of penetration of the water (w) into the nonpolar phase by about 5 $\AA$. Unlike the case of a hard or rigid wall [50, 51, 52, 53], where large density fluctuations are seen in the water density near the interface, the present results show a relatively flat profile with the water quicky reaching its bulk density (≈ 1.0 g/cm^3). This behavior is similar to that seen at the interface between water and a bulk hydrocarbon liquid [54], and is likely due to a "smearing-out" effect of the water density profile due to undulatory fluctuations in the surface of the hydrocarbon phase [55, 56]. A slight separation in the H and O profiles can also be seen, which indicates the existence of some degree of orientational ordering of the water molecules near the interface.

In the mixed solvent systems, there is a striking segregation of the organic (o) component at the interface. This build-up of the organic component excludes water from the interface, as shown by the location of the Gibbs dividing surface z_G, defined by the condition

$$\int_0^{z_G} \rho_w(z)dz = -\int_{z_G}^{z_C} (\rho_w(z) - \rho_{w,C})dz, \tag{19}$$

where ρ_w is the number density of water and $\rho_{w,C}$ is the density of the water at the center of the pore, z_C. The values of z_G are 10.2 $\AA$, 12.6 $\AA$, and 14.7 $\AA$ for the pure water, methanol/water, and acetonitrile/water systems, respectively. In the water/methanol system, the alcohol concentration near the chain surfaces is nearly twice its value in the bulk. One can also clearly see a preferential orientation of the methanol in this region, as has been previously noted [30], with the methyl group pointing toward the hydrocarbon phase while the hydroxyl group maximizes its H-bonding interactions with the water. The layering of the organic phase near the interfaces is qualitatively similar in the acetonitrile/water system, where it is even more pronounced. Here the peak interfacial concentration of acetonitrile exceeds twice the value near the center of the pore. Both the acetonitrile and the methanol penetrate into the hydrocarbon phase to approximately the same degree, with primary and secondary peaks in the densities occuring at the surface and several $\AA$ into the surface. Unlike the methanol/water system, where the presence of the methanol tends to pull some of the water into the hydrocarbon phase, in the acetonitrile/water system interfacial acetonitrile tends to exclude water from the interface because of the much weaker acetonitrile-water interactions. Additionally, the density profiles for acetonitrile do not indicate a significant amount of orientational ordering of the acetonitrile molecules at the interface.

The total site number densities along the z coordinate (Figure 6) reveal a sharp interface in the pure water system which becomes less sharp in the water/methanol system and is quite diffuse in the acetonitrile/water system. These data also indicate the presence of small density peaks due to alkyl chain layering.

4.2 Energy profiles

In figures 7 - 9 we plot the pairwise energy contributions from the LJ, Coulombic, and intramolecular interactions as a function of distance along the z coordinate. The intra and intermolecular chain-chain interactions reflect the tendency for the sites of the chains to arrange into two loosely defined layers at a position near the wall, where the first sites of the chains are constrained via the spring interaction, and at a distance 3 $\AA$ to 4 $\AA$ from

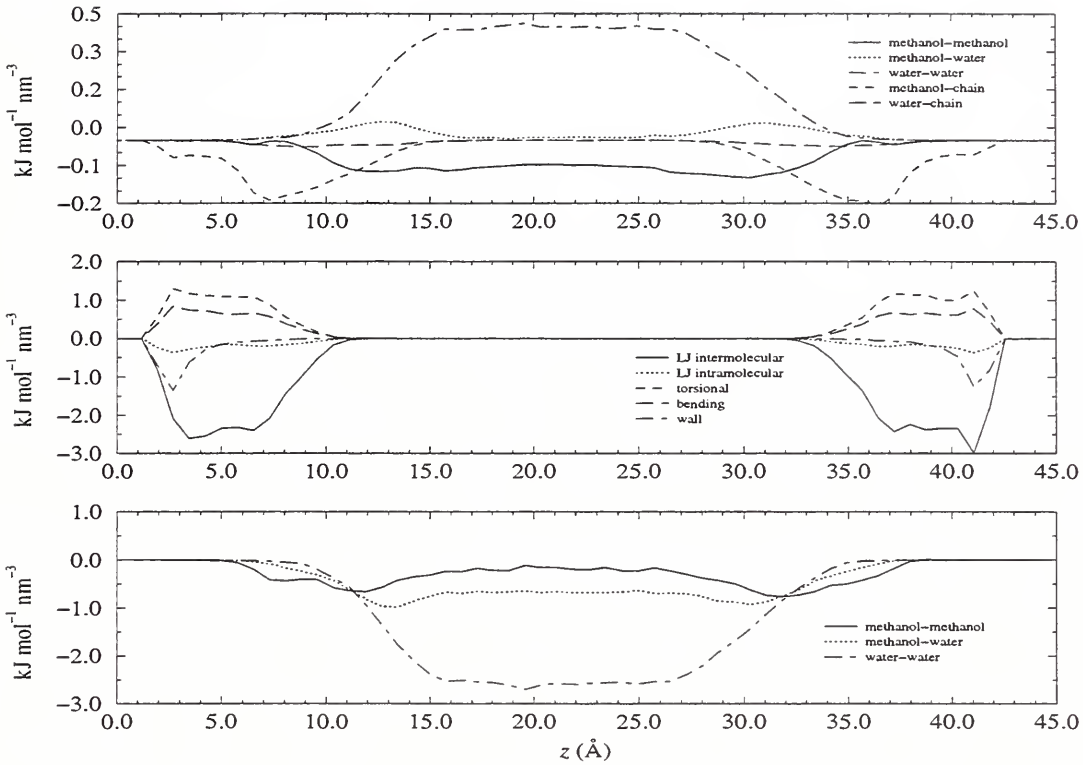

Figure 8: Energy density from various sources as a function of z for the methanol/water system. (see Legend for Figure 7)

the interface. This type of layering in the hydrocarbon phase has also been seen in C_{18} stationary phases [30], and is expected to present a free energy barrier which to some degree inhibits penetration into the hydrocarbon phase by a solute. The interaction between the water and the alkyl chains is weak and appears to be diminished by the presence of the organic components. In all three systems, the water-water interactions are characterized by a balance between the Coulombic attraction of the hydrogen bonding and the overlap LJ OO energy. In the pure water system, the total configurational energy at the center of the pore is -41.1 kJ/mol, which is close to the value for bulk SPC water. The repulsive LJ OO interaction for the methanol-water pairs is partially offset by attractive dispersion between the water oxygen and the methyl group. The methanol-water interaction is largely dominated by hydrogen bonding, while the much weaker acetonitrile-water interaction appears to be dominated slightly by dispersion interactions and weak Coulombic interactions. The methanol-methanol energies are characterized by a combination of hydrogen-bonding with some dispersion interactions while in the acetonitrile-acetonitrile interactions both dispersion and Coulombic interactions appear to play equally important roles. The more pronounced layering of the organic co-solvent in the acetonitrile/water system is therefore due to both weaker acetonitrile-water interactions and stronger acetonitrile-chain interactions, the latter being about twice the magnitude of the corresponding methanol-chain pairwise energies. These results are in agreement with previous notions concerning differences between acetonitrile/water and methanol/water mobile phases in the solvation of the stationary phase by the organic component [13]. However, we note that with the present mostly aqueous solvents, the organic component cannot be said to *solvate* the alkyl chains to any appreciable extent. Instead, there is considerable *wetting* of the alkyl chain surface by the organic co-solvent, although solvation is to be expected with mobile phases which are organic-rich [13, 14].

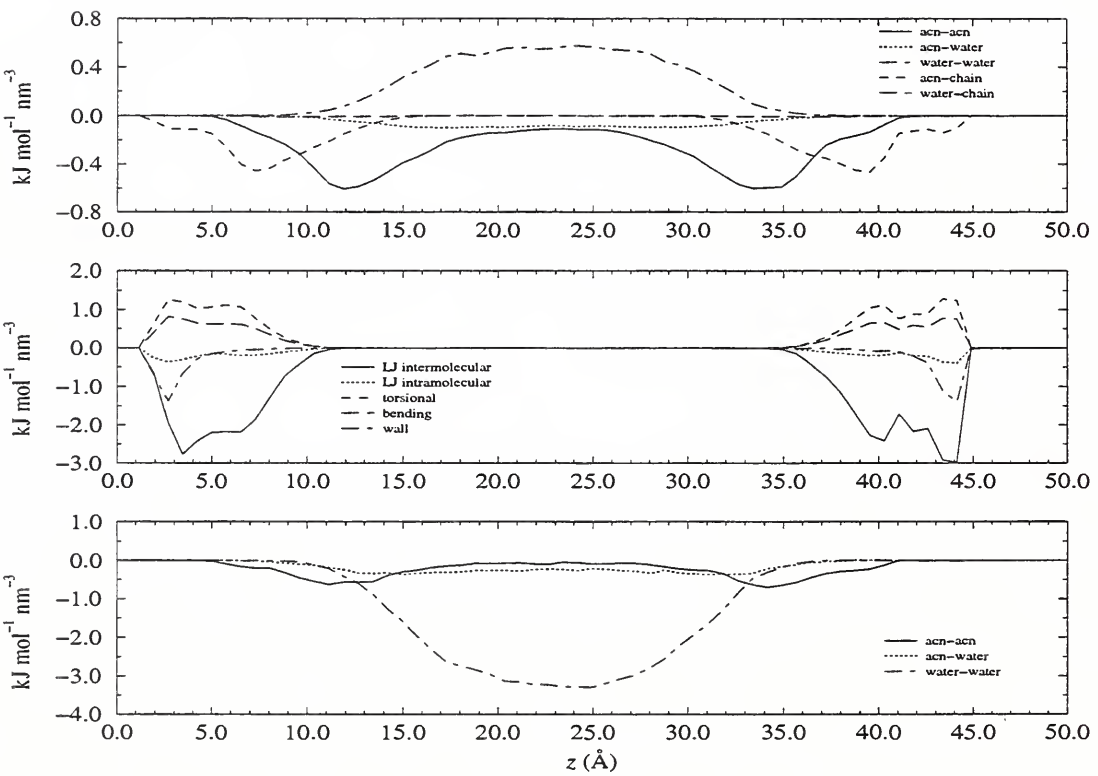

Figure 9: Energy density from various sources as a function of z for the acetonitrile/water system. (see Legend for Figure 7)

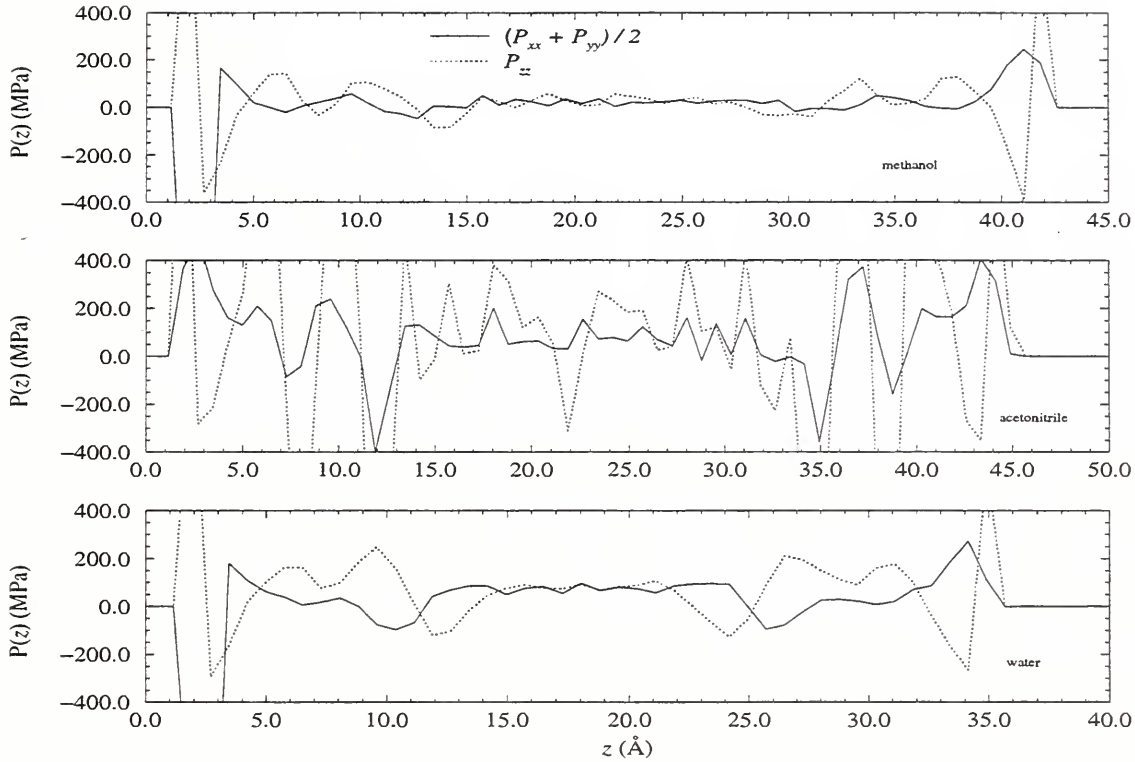

Figure 10: Components of the pressure tensor as a function of z distance for the methanol/water sytem (TOP), acetonitrile/water system (MIDDLE) and pure water system (BOTTOM).

4.3 Pressure profiles

The diagonal components of the pressure tensor are plotted as a function of z in Figure 10. In principle, if bulk-like behavior were observed on both sides of the interface, one could use these data to calculate a surface tension at the water/chain interface, information which would be of relevance to the solute transfer mechanism [9, 14]. However, although bulk-like behavior is seen in the center of the pore, where $P_{xx} \approx P_{yy} \approx P_{zz}$, this is not the case in the alkyl chain phase due to both the effects of the interface as well as wall and spring interactions with the chains. In any case, the statistical noise in the data prevents all but the qualitative observation that the surface tension decreases in the order of the water, methanol, acetonitrile systems.

4.4 Chain structure

An important question related to the retention mechanism in RPLC is the effect of different mobile phases on the ordering of the stationary phase. The expectation has been that disordered or folded states predominate with poor chain solvents such as water, while solvation of the chains with an organic component favors chain extension and ordering [26, 57, 58]. Three quantities which give a measure of the chain structure from the simulations are the distribution of the angle χ, defined as

$$\cos\chi \equiv \hat{\mathbf{r}}_{18} \cdot \hat{\mathbf{z}}, \tag{20}$$

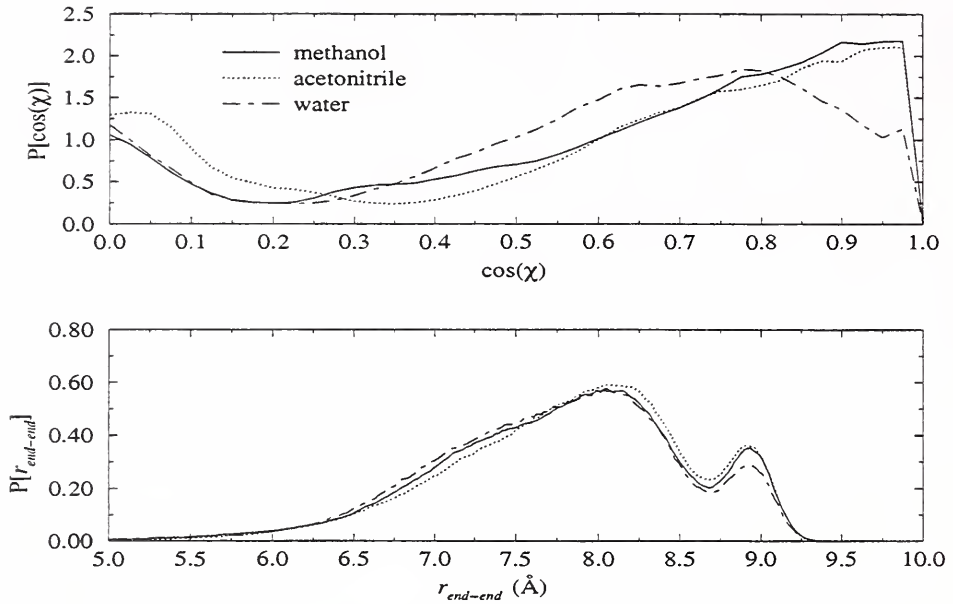

Figure 11: Probability density of chain-wall normal angle (TOP) and chain end-end distance (BOTTOM) for different systems.

where $\mathbf{r}_{18} = \mathbf{r}_8 - \mathbf{r}_1$ and $\hat{\mathbf{z}}$ is a unit normal to the wall, the distribution of the end-end distance of the alkyl chains, and the center of mass of the hydrocarbon layer,

$$\langle z \rangle \equiv \int_0^{zc} z\rho_s(z)dz \Big/ \int_0^{zc} \rho_s(z)dz, \tag{21}$$

where $\rho_s(z)$ is the total number density of the methyl sites of the chains. The distributions are compared in Figure 11 for the three systems. We note first that the values of χ are bimodally distributed with a tendency for the chains to either extend away from the surface or to lie nearly flat in an orientation parallel to the walls. Apparently, the interaction of the chains with the wall potential begins to predominate when the chains begin to lie close to the wall. Given the rather limited flexibility in C_8 chains there is little difference in the results for the different systems, particularly since the hydrophobic nature of the solvent has not changed greatly among the three systems. The statistically indistinguishable values of $\langle z \rangle$ support this observation, being 5.92 $\AA$, 5.97 $\AA$, and 6.00 $\AA$ for the water, acetonitrile/water, and methanol/water sytems, respectively. From the distributions of χ, we can tentatively conclude that the occurrence of nearly straight chains perpendicular to the walls is slightly diminished in the pure water systems relative to the others. Such distinctions are likely to be much more pronounced in systems having longer alkyl chains such as C_{18}. We are currently performing a detailed analysis of the effect of solvent composition on the C_{18} conformational order. Interestingly, Sander *et al.* [26], using infrared spectrometry, found marked differences in the C_{18} alkyl chain conformation for dry RPLC packings compared to those in the presence of mobile phase. However, they did not detect any significant changes in the IR spectra with mobile phase compositions in organic-rich (70 % to 100 %) methanol/water solutions.

The $r_{end-end}$ distribution is also bimodal with a peak at about 8.9 $\AA$ corresponding to the nearly all-trans configuration. The broad distribution in $r_{end-end}$ indicates numerous gauche defects in the majority of the chains. For C_8 chains at a surface concentration of

about 5.1 μmol/m^2 in an environment of pure water and in water-rich aqueous methanol and aqueous acetonitrile, the overall picture is one in which the chains are largely disordered with some lying flat against the surface, while the majority are oriented with χ greater than about 60°. The presence of 30 mole % methanol or acetonitrile changes this picture only slightly (compared to the pure water system), with some evidence for a small increase in chain extension.

4.5 Solvent orientation

The average orientation of the solvent as a function of distance in the z direction has been examined by defining

$$\cos\beta \equiv \hat{d} \cdot \hat{z}, \qquad \cos\gamma \equiv \hat{b} \cdot \hat{z}, \tag{22}$$

where $\hat{d}$ is the unit dipole vector and $\hat{b}$ is a unit bond vector pointing from the oxygen to the methyl group on a methanol molecule. $\hat{z}$ is a unit normal to the wall pointing in the positive direction so that the functions $\cos\beta z$ and $\cos\gamma(z)$ are expected to be rotationally symmetric about z_C. These results are plotted in Figure 12. In the center, the averages of both $\cos\beta$ and $\cos\gamma$ are zero, indicating no preferential orientation of the molecules with respect to the walls. The data become noisier near the ends where the statistics become worse. For the pure water system, the orientation of the water dipole moments near the surface of the hydrocarbon phase is nearly identical with the results for the free interface of pure water [59]. In this case, the sign of $\cos\beta$ changes at the location of the Gibbs dividing surface, where there is a slight tendency for orientations of the dipole moment toward the bulk for $z > z_G$ while the reverse is true for $z < z_G$. For the mixed-solvent systems, the water dipole moment points more toward the bulk, on average, on both sides of the Gibbs dividing surface in the methanol/water system. This behavior is similar to that seen for free surfaces of water in the presence of sub-monolayer coverages of phenol [59]. The water in the acetonitrile/water system shows qualitatively different behavior, with the orientation of the water dipole moments being always toward the walls, with the possible exception of the most deeply penetrating water.

The onset of orientational preference of the methanol begins when the number density starts to increase near the interface. These results show that the alignment of the methyl-oxygen bond with the z axis becomes more and more pronounced as the methanol penetrates deeper into the alkyl chains. The behavior of the acetonitrile molecules is more complex. There appears to be little orientational preference of the acetonitrile molecules either in the bulk or within the organic-rich surface layers. Near the inner edges of these layers, the molecules tend to orient their methyl groups toward the walls, while near the outer edges of these layers, the molecules tend to point their methyl groups toward the water-rich center, which seems to be a counterintuitive result.

4.6 Free energy profile

The residual Helmholtz free energy profile of a methane solute ($\sigma = 0.373$ nm, $\epsilon/k_b = 147.5$ K) in the acetonitrile/water system has been estimated using equation (18) by performing a series of simulations with the starting configuration taken from the ending configuration of the acetonitrile/water simulation discussed above. Two solutes were utilized in each simulation, one constrained via equation (17) at a position $z_\circ$ while the other was constrained to be at $L - z_\circ$. A total of 11 simulations of lengths > 90 ps were run, with the results from

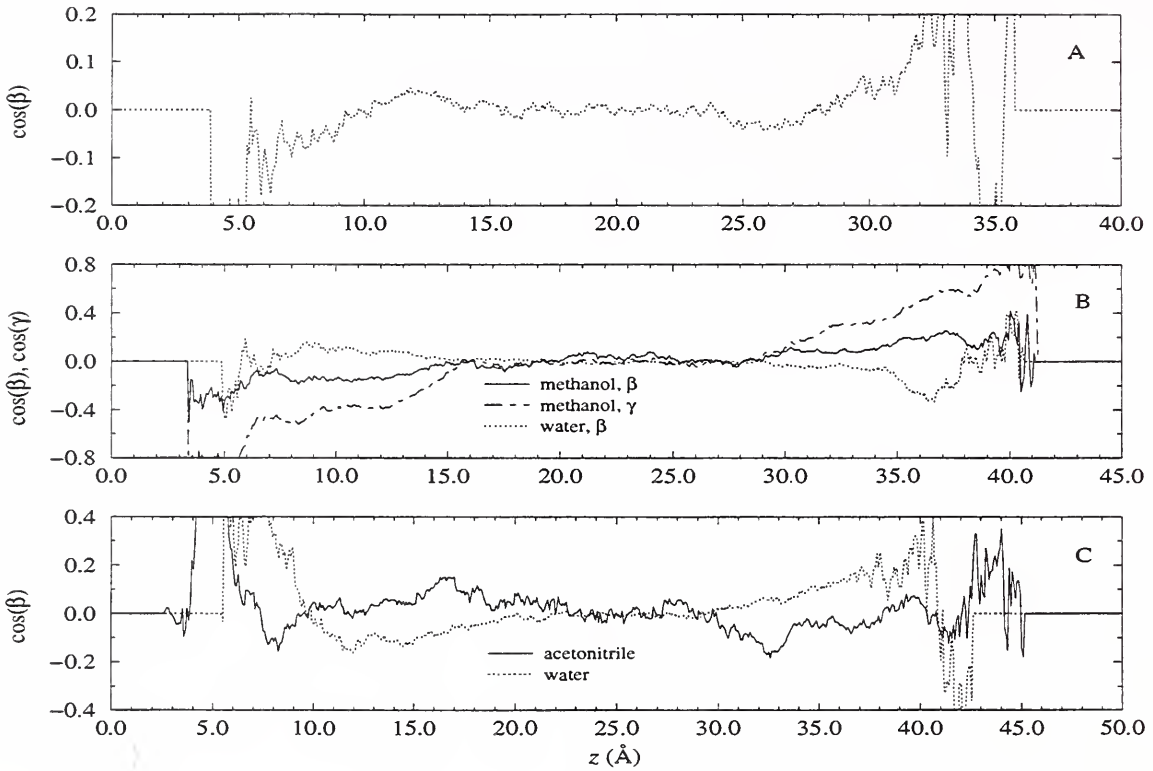

Figure 12: Average dipole-wall and bond vector-wall angles as a function of distance in the z direction, pure water (A), methanol/water (B), and acetonitrile/water (C) systems.

each z window being shifted so that the endpoints of a window matched the endpoints of the neighboring windows. These results are displayed in Figure 13 for the solute at $z_\circ$ (solid line) and at $L - z_\circ$ (dotted line), along with the full density profile for comparison. The qualitative behavior of both solutes is similar, although they do not follow exactly the same path, (particularly when the solute resides in the hydrocarbon phase), and there is considerable noise in the results. We can, however, note several features of these free energy profile estimates. In particular, there appears to be a small free energy barrier at about $z = 17\mathring{A}$, corresponding to the position of the outer edge of the acetonitrile-rich layer at the hydrocarbon surface, a finding which is similar to that seen by Klatte and Beck in the methanol/water system at the same bulk mole fraction of organic co-solvent [30]. Once the solute enters the acetonitrile-rich layer at the interface, the free energy drops continuously. At the location of the second acetonitrile peak at about 8 $\mathring{A}$ from the wall, the results for the two different solutes are ambiguous, as the free energy continues to drop for one while leveling off for the other solute. In any case, a substantial portion of the total free energy driving force for a methane solute in the acetonitrile system occurs in the organic-rich layer adsorbed to the hydrocarbon phase, a result which is quite similar to that found previously for a methanol/water/C_{18} system. On the basis of the present results, we are therefore unable to identify any distinctly different behavior of a simple spherical solute in the acetonitrile/water system as compared to the methanol/water system, at least at the current composition conditions. We are currently planning investigations of free energy profiles for molecular solutes, such as benzene, with concurrent estimates of the solute energy and entropy profiles as well.

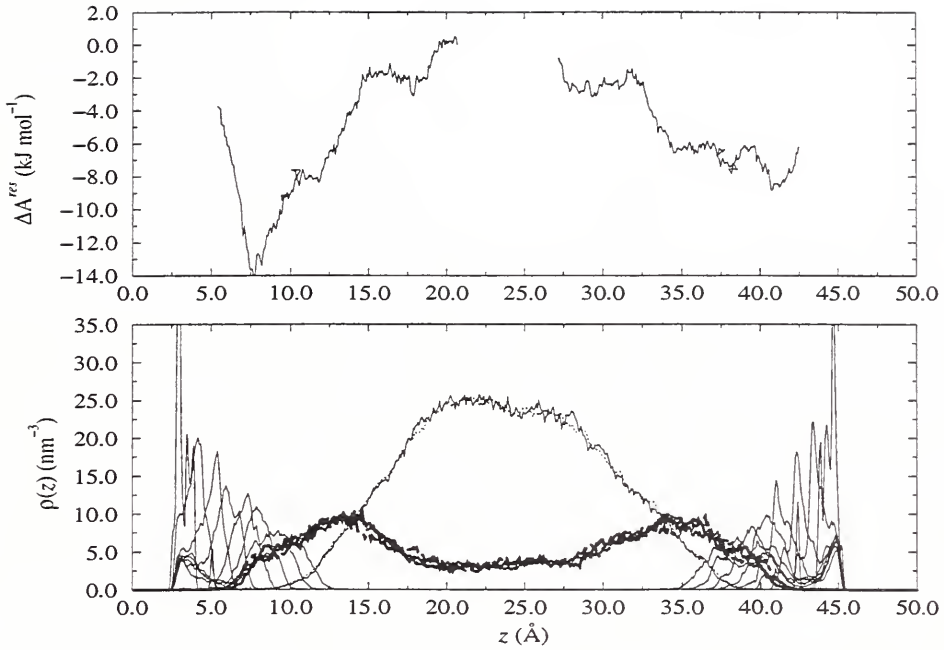

Figure 13: (TOP) Change in residual Helmholtz free energy of a methane solute with position along the z coordinate. (BOTTOM) Full density profiles for the acetonitrile/water system. (See legend to figure 3)

5 Conclusions

In this report we have outlined a molecular dynamics model for the study of interphases in reversed phase liquid chromatography using molecular dynamics simulation. The approach adopted here is one in which the model system is somewhat idealized but, we believe, still captures the essential features of the real system. Further, we have treated the long-ranged electrostatic interactions rigorously with an Ewald sum and derived expressions for the Coulombic contribution to the pressure tensor. The use of an Ewald sum to rigorously deal with the long-ranged Coulombic interactions is very expensive computationally. However, spherical truncation of these interactions can have a significant effect on the computed results. This effect is illustrated in Figure 14, in which the density profiles are compared in the methanol/water system for the Ewald sum and for spherical cutoff based on center-of-mass distances. For the latter case, the sharpness of the interface is underestimated while the layering of the methanol is overestimated.

Some features of the model system remain arbitrary, such as the parameters and form of the wall potential and the chain linkage to the wall. However, these simplifications are likely to have little impact on the calculation of the solute free energy profiles, which give a detailed picture of the driving forces behind the retention process.

References

[1] J. G. Dorsey and K. A. Dill. Chem. Rev., 89 (1989) 331.

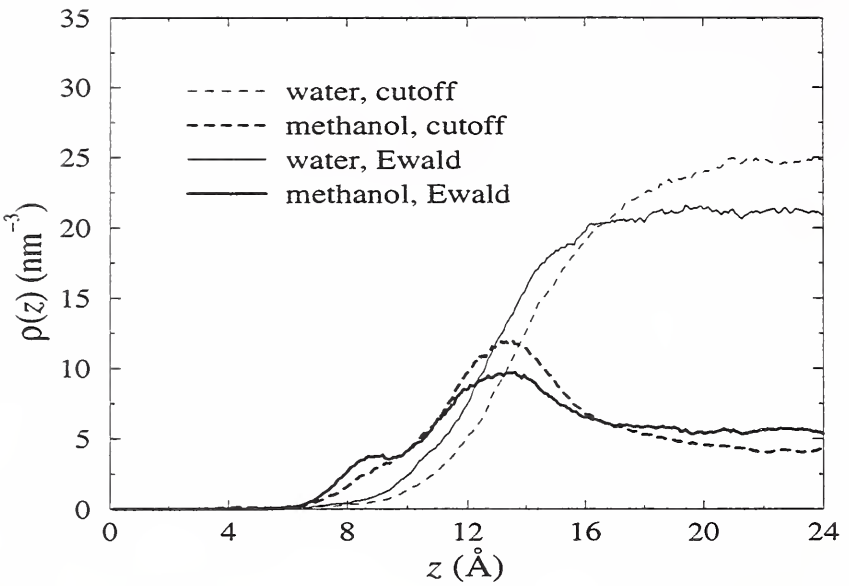

Figure 14: Comparison of density profiles for the oxygen site of water and methanol with spherical truncation of Coulombic interactions and Ewald sum.

[2] P. W. Carr, J. Li, A. J. Dallas, D. I. Eikens and L. C. Tan. Journal of Chromatography A, 656 (1993) 113.

[3] G. E. Berendsen and L. D. Galan. Journal of Chromatography, 196 (1980) 21.

[4] J. Kohler, D. B. Chase, R. D. Failee, A. J. Vega and J. J. Kirkland. Journal of Chromatography, 352 (1986) 275.

[5] P. Roumeliotis and K. K. Unger. Journal of Chromatography, 149 (1978) 211.

[6] J. J. Kirkland, J. L. Glajch and R. D. Farbe. Analytical Chemistry, 61 (1989) 2.

[7] C. H. Lochmüller, A. S. Colborn, M. L. Hunnicutt and J. M. Harris. Analytical Chemistry, 55 (1983) 1344.

[8] J. A. Marqusee and K. A. Dill. Journal of Chemical Physics, 85 (1986) 434.

[9] C. Horváth, W. Melander and I. Molnár. Journal of Chromatography, 125 (1976) 129.

[10] K. A. Dill. Journal of Physical Chemistry, 91 (1987) 1980.

[11] K. B. Sentell and J. G. Dorsey. Journal of Chromatography, 461 (1989) 193.

[12] A. Alvarez-Zepeda, B. N. Barman and D. E. Martire. Analytical Chemistry, 64 (1992) 1978.

[13] D. M. Bliesner and K. B. Sentell. Analytical Chemistry, 65 (1993) 1819.

[14] J. M. E. Montgomery, M. A. Green and M. J. Wirth. Analytical Chemistry, 64 (1992) 1170.

[15] S. A. Wise, W. J. Bonnett, F. R. Guenther and W. E. May. Journal of Chromatogr. Sci., 19 (1981) 457.

[16] S. A. Wise and L. C. Sander. Journal of High Resolut. Chromatogr. Chromatogr. Commun., 8 (1985) 248.

[17] Y. C. Guillaume and C. Gunichard. Analytical Chemistry, 68 (1996) 2869.

[18] A. M. Stalcup, D. E. Martire and S. A. Wise. Journal of Chromatography A, 442 (1988) 1.

[19] S. Balakrishnan and A. J. Easteal. Aust. J. Chem., 34 (1981) 943.

[20] P. W. Carr, R. M. Doherty, M. J. Kamlet, R. W. Taft, W. Melander and C. Horvath. Analytical Chemistry, 58 (1986) 2674.

[21] B. P. Johnson, M. G. Khaledi and J. G. Dorsey. Anaytical Chemistry, 58 (1986) 2354.

[22] T. Hanai, A. Jukurogi and J. Hubert. Chromatographia, 19 (1984) 266.

[23] K. L. Rowlen and J. M. Harris. Analytical Chemistry, 63 (1991) 964.

[24] Y. Marcus and Y. Migron. Journal of Physical Chemistry, 95 (1991) 400.

[25] C. G. Gray and K. E. Gubbins. Theory of Molecular Fluids. Vol. I. Clarendon Press, Oxford, (1984).

[26] L. C. Sander, J. B. Callis and L. R. Field. Analytical Chemistry, 55 (1983) 1068.

[27] L. A. Cole and J. G. Dorsey. Analytical Chemistry, 64 (1992) 1317.

[28] L. A. Cole, J. G. Dorsey and K. A. Dill. Analytical Chemistry, 64 (1992) 1324.

[29] E. D. Katz, K. Ogan and R. P. W. Scott. Journal of Chromatography, 352 (1986) 67.

[30] S. J. Klatte and T. L. Beck. Journal of Physical Chemistry, 100 (1996) 5931.

[31] I. K. Snook and W. van Megen. Journal of Chemical Physics, 72 (1980) 2907.

[32] J.-P. Ryckaert and A. Bellemans. Discuss. Faraday Soc., 66 (1978) 95.

[33] J. Böcker, M. Schlenkrich, P. Bopp and J. Brickmann. Journal of Physical Chemistry, 96 (1992) 9915.

[34] H. Bekker, H. J. C. Berendsen and W. F. van Gunsteren. Journal of Computational Chemistry, 16 (1995) 527.

[35] H. J. C. Berendsen, J. P. M. Postma, W. F. van Gunsteren and J. Hermans. In Intermolecular Forces (B. Pullman, ed.), D. Reidel. 1981 pp. 331–342, pp. 331–342.

[36] M. E. van Leeuwen. Molecular simulation of the phase behaviour of polar fluids. Ph.D. Thesis, Universiteit Utrecht, the Netherlands.

[37] D. M. F. Edwards, P. A. Madden and I. R. McDonald. Molecular Physics, 51 (1984) 1141.

[38] J. T. Slusher and P. T. Cummings. Molecular Simulation, 18 (1996) 213.

[39] D. Beeman. Journal of Computational Physics, 20 (1976) 130.

[40] S. Melchionna, G. Ciccotti and B. L. Holian. Molecular Physics, 78 (1993) 533.

[41] Y.-H. Rhee, J. W. Halley, J. Hautman and A. Rahman. Physical Review B, 40 (1989) 36.

[42] E. R. Smith. Molecular Physics, 65 (1988) 1089.

[43] A. H. Widmann and D. B. Adolf. Comp. Phys. Comm., 107 (1997) 167.

[44] J. Hautman and M. L. Klein. Molecular Physics, 75 (1992) 379.

[45] J. Leckner. Physica A, 176 (1991) 485.

[46] D. M. Heyes, M. Barber and J. H. R. Clarke. J. Chem. Soc. Faraday Trans. II, 73 (1977) 1485.

[47] M. P. Allen and D. J. Tildesley. Computer Simulation of Liquids. Oxford University Press, New York, (1987).

[48] L. C. Sander and S. A. Wise. In Retention and Selectivity in Liquid Chromatography (R. M. Smith, ed.), Elsevier Science, vol. 57. 1995 p. 337, p. 337.

[49] D. Chandler. Introduction to modern statistical mechanics. Oxford University Press, NY, (1987).

[50] B. Jönsson. Chem. Phys. Lett., 82 (1981) 520.

[51] M. Marchesi. Chem. Phys. Lett., 97 (1983) 224.

[52] C. Y. Lee and J. A. McCammon. J. Chem. Phys., 80 (1984) 4448.

[53] N. I. Christou, J. S. Whitehouse, D. Nicholson and N. G. Parsonage. Mol. Phys., 55 (1985) 397.

[54] D. Michael and I. Benjamin. J. Phys. Chem., 99 (1995) 1530.

[55] I. Benjamin. J. Chem. Phys., 97 (1992) 1432.

[56] A. Pohorille and M. A. Wilson. J. Molec. Struct. (Theochem), 284 (1993) 271.

[57] R. K. Gilpin and J. A. Squires. J. Chromatograph. Sci., 19 (1981) 195.

[58] R. K. Gilpin, M. E. Gangoda and A. E. Krishen. J. Chromatograph. Sci., 20 (1982) 345.

[59] V. P. Sokhan and D. J. Tildesley. Mol. Phys., 92 (1997) 625.

[60] F. B. Hildebrand. Advanced Calculus for Applications, 2^{nd} Ed. Prentice-Hall, Inc., NJ, (1976).

[61] M. Abramowitz and I. R. Stegun (eds.). Handbook of mathematical functions. U.S. Dept. of Commerce, D.C., (1964).

[62] S. Nosé and M. L. Klein. Molecular Physics, 50 (1983) 1055.

[63] D. Brown and S. Neyertz. Molecular Physics, 84 (1995) 577.

6 Appendix

The Coulombic energy is given by a sum of real-space, reciprocal-space, constant, self, and multipole energies, $U^C = U_R + U_F + U_{cons} + U_{self} + U_m$ where

$$U_R = \sum_i \sum_{j>i} \sum_\alpha \sum_\beta \sum_\nu q_{i\alpha} q_{j\beta} \left\{ \frac{1}{r_{i\alpha j\beta,\nu}} - F_1(\alpha; s_{i\alpha j\beta,\nu}) \right\}, \tag{23}$$

$$U_F = \frac{\pi}{A} \sum_{\mathbf{G}\neq 0} A_G \left|G_\Sigma\right|^2, \tag{24}$$

$$U_{cons} = \frac{1}{2} \sum_i \sum_\alpha q_{i\alpha}^2 \sum_{\nu\neq 0} \left\{ \frac{1}{\nu} - F_1(\alpha; \nu) \right\}, \tag{25}$$

$$U_{self} = -\frac{1}{2} \sum_i \sum_\alpha q_{i\alpha}^2 \int_0^\infty e^{-(\alpha G)^3} dG - \sum_i \sum_\alpha \sum_{\beta>\alpha} q_{i\alpha} q_{i\beta} F_1(\alpha; s_{i\alpha i\beta}), \tag{26}$$

$$U_m = \sum_i \sum_{j>i} \sum_\alpha \sum_\beta q_{i\alpha} q_{j\beta} \left\{ -\frac{1}{2} \left(\sum{}' \frac{1}{\nu^3} \right) z_{i\alpha j\beta}^2 + \right.$$
$$\left. \frac{3}{8} \left(\sum{}' \frac{1}{\nu^5} \right) z_{i\alpha j\beta}^4 - \frac{9}{8} \left(\sum{}' \frac{1}{\nu^5} \right) z_{i\alpha j\beta}^2 s_{i\alpha j\beta}^2 \right\} \tag{27}$$

with

$$F_1(\alpha; \xi) = \int_0^\infty J_0(G\xi) e^{(\alpha G)^3} dG, \tag{28}$$

$$A_G = \frac{e^{-(\alpha G)^3}}{G}, \tag{29}$$

$$\left|G_\Sigma\right|^2 = \left[\left(\sum_i \sum_\alpha q_{i\alpha} \cos(\mathbf{G} \cdot \mathbf{s}_{i\alpha}) \right)^2 + \left(\sum_i \sum_\alpha q_{i\alpha} \sin(\mathbf{G} \cdot \mathbf{s}_{i\alpha}) \right)^2 \right], \tag{30}$$

$$\sum{}' \frac{1}{\nu^n} = \sum_{\{all\ \ \nu\}} \frac{1}{\nu^n} - \sum_{\{\nu_x, \nu_y \leq \nu_c\}} \frac{1}{\nu^n}, \quad \nu = L\mathbf{n}, \quad \mathbf{n} = (n_x, n_y), \quad n_x, n_y = 1, 2, 3, \ldots \tag{31}$$

where $q_{i\alpha}$ is the dimensionless fractional charge on site α of molecule i, $L = L_x = L_y$, $A = L^2$, ν is a lattice vector, ν_c is the lattice vector cutoff, J_0 is the zeroth order Bessel function of the first kind [60], and $\mathbf{G}$ are reciprocal lattice vectors in the $x - y$ plane. In the above equations the factor $1/4\pi\epsilon_\circ$ has been omitted. $\mathbf{s}$ and $\mathbf{z}$ are the $x - y$ and z components of the positions. The forces are obtained straightforwardly by differentiation:

$$\mathbf{F}_{Ri\alpha j\beta}^s = \sum_i \sum_{j>i} \sum_\alpha \sum_\beta \sum_\nu q_{i\alpha} q_{j\beta} \left\{ \frac{1}{r_{i\alpha j\beta,\nu}^3} - F_2(\alpha; s_{i\alpha j\beta,\nu}) \right\} \mathbf{s}_{i\alpha j\beta,\nu} \tag{32}$$

$$\mathbf{F}_R^z = \sum_i \sum_{j>i} \sum_\alpha \sum_\beta \sum_\nu q_{i\alpha} q_{j\beta} \frac{\mathbf{z}_{i\alpha j\beta}}{r_{i\alpha j\beta,\nu}^3} \tag{33}$$

$$\mathbf{F}_m^s = \sum_i \sum_{j>i} \sum_\alpha \sum_\beta q_{i\alpha} q_{j\beta} \frac{9}{4} \left(\sum{}' \frac{1}{\nu^5} \right) z_{i\alpha j\beta}^2 \mathbf{s}_{i\alpha j\beta} \tag{34}$$

$$\mathbf{F}_m^z = \sum_i \sum_{j>i} \sum_\alpha \sum_\beta q_{i\alpha} q_{j\beta} \left\{ \sum{}' \frac{1}{\nu^3} - \frac{3}{2} \left(\sum{}' \frac{1}{\nu^5} \right) z_{i\alpha j\beta}^2 + \frac{9}{4} \left(\sum{}' \frac{1}{\nu^5} \right) s_{i\alpha j\beta}^2 \right\} \mathbf{z}_{i\alpha j\beta} \tag{35}$$

$$\mathbf{F}_F = \frac{2\pi}{A} \sum_{\mathbf{G}\neq 0} A_G \mathbf{G} \left[\left(\sum_i \sum_\alpha \cos(\mathbf{G} \cdot \mathbf{s}_{i\alpha}) \right) q_{i\alpha} \sin(\mathbf{G} \cdot \mathbf{s}_{i\alpha}) - \right.$$

$$\left(\sum_i \sum_\alpha \sin(\mathbf{G}\cdot\mathbf{s}_{i\alpha})\right) q_{i\alpha}\cos(\mathbf{G}\cdot\mathbf{s}_{i\alpha})\Bigg], \quad (36)$$

where

$$F_2(\alpha;\xi) = \frac{1}{\xi}\int_0^\infty J_1(G\xi)Ge^{-(\alpha G)^3}dG$$

and J_1 is the first order Bessel function of the first kind [60]. In practice, the Bessel functions J_0 and J_1 are computed using polynomial representations found in reference [61]. After choosing an appropriate value for the convergence parameter α, the functions F_1 and F_2 are tabulated and their values interpolated linearly during the program execution.

In the molecular formulation, the Coulombic contribution to the pressure tensor is given by $\mathbf{P}^C = \mathbf{P}^R + \mathbf{P}^F + \mathbf{P}^m + \mathbf{P}^{cons}$, where, following the development in the 3DP formulation of Nosé and Klein [62] and Brown and Neyertz, [63], we have, for the (α,β) component

$$V\mathbf{P}^R_{\alpha\beta} = \sum_i\sum_{j>i}\sum_\gamma\sum_\mu\sum_\nu (\mathbf{R}_{ij,\nu})_\alpha \left(\mathbf{F}^R_{i\gamma j\mu,\nu}\right)_\beta \quad (37)$$

$$V\mathbf{P}^F_{\alpha\beta} = \frac{\pi}{A}\sum_{\mathbf{G}\neq\mathbf{0}} A_G\left(\delta_{\alpha\beta} - (3\alpha^3 G + \frac{1}{G^2})G_\alpha G_\beta\right)|G_\Sigma|^2$$
$$+\frac{2\pi}{A}\sum_{\mathbf{G}\neq\mathbf{0}}\Bigg\{A_G\Bigg[\left(\sum_i\sum_\gamma q_{i\gamma}\sin(\mathbf{G}\cdot\mathbf{s}_{i\gamma})\right)\left(\sum_i\sum_\gamma q_{i\gamma}\cos(\mathbf{G}\cdot\mathbf{s}_{i\gamma})G_\alpha(d_{i\gamma})_\beta\right)$$
$$-\left(\sum_i\sum_\gamma q_{i\gamma}\cos(\mathbf{G}\cdot\mathbf{s}_{i\gamma})\right)\left(\sum_i\sum_\gamma q_{i\gamma}\sin(\mathbf{G}\cdot\mathbf{s}_{i\gamma})G_\alpha(d_{i\gamma})_\beta\right)\Bigg]\Bigg\} \quad (38)$$

$$V\mathbf{P}^{cons}_{\alpha\beta} = \frac{1}{2}\sum_i\sum_\gamma q^2_{i\gamma}\sum_{\nu\neq\mathbf{0}}\left\{\frac{\nu_\alpha\nu_\beta}{\nu^3} - \nu_\alpha\nu_\beta F_2(\alpha;\nu)\right\} \quad (39)$$

$$V\mathbf{P}^m_{\alpha\beta} = \sum_i\sum_{j>i}\sum_\gamma\sum_\mu (\mathbf{R}_{ij})_\alpha\left(\mathbf{F}^m_{i\gamma j\mu}\right)_\beta$$
$$+\sum_i\sum_{j>i}\sum_\gamma\sum_\mu q_{i\gamma}q_{j\mu}\Bigg\{\frac{-3}{2}\left(\sum{}'\frac{\nu_\alpha\nu_\beta}{\nu^5}\right)z^2_{i\gamma j\mu}$$
$$+\frac{15}{8}\left(\sum{}'\frac{\nu_\alpha\nu_\beta}{\nu^7}\right)z^4_{i\gamma j\mu} - \frac{45}{8}\left(\sum{}'\frac{\nu_\alpha\nu_\beta}{\nu^7}\right)z^2_{i\gamma j\mu}s^2_{i\gamma j\mu}\Bigg\} \quad (40)$$

where $\delta_{\alpha\beta}$ is the Kronecker delta.

The atomic formulation of the pressure tensor includes the intramolecular forces, and its Coulombic contribution is the same as the molecular pressure tensor, with $(R_{ij,\nu})_\alpha$ and $(R_{ij})_\alpha$ replaced by $(r_{i\gamma j\mu,\nu})_\alpha$ and $(r_{i\gamma j\mu})_\alpha$, and dropping the second term in $P^F_{\alpha\beta}$. Furthermore, by symmetry, the off-diagonal terms in $P^{cons}_{\alpha\beta}$ and in the second term of $P^m_{\alpha\beta}$ are zero.

For spherical ions, we also have the well-known result that $P^C = \frac{1}{3}\mathrm{Tr}(P^C) = \frac{1}{3V}\langle U^C\rangle$, which provides a convenient check for the above expressions. A test calculation of 256 KCl ions yielded agreement in the last expression to within numerical error.

The total pressure tensor in the 'atomic' framework is given by

$$\mathbf{P} = \mathbf{P^C} + \mathbf{P}^{LJ} + \mathbf{P}^{tors} + \mathbf{P}^{bend} + \mathbf{P}^{LJ,intra} + \mathbf{P}^{constraint} + \mathbf{P}^{wall} + \mathbf{P}^{spring}, \quad (41)$$

where $\mathbf{P}^{LJ}$ is the intermolecular contribution due to Lennard-Jones interactions, $\mathbf{P}^{tors}$, $\mathbf{P}^{bend}$, and $\mathbf{P}^{LJ,intra}$ are contributions from the intramolecular potential of the chains, $\mathbf{P}^{constraint}$ is the constraint force contribution, and $\mathbf{P}^{wall}$ and $\mathbf{P}^{spring}$ are contributions from the wall and the spring attached to the first site of the C_8 chains.